PMN-PT Single Crystal Ultrasonic Transducer with Half-concave Geometric Design for IVUS Imaging

*Chunlong FEI[†a], Yaoheng YANG[†b], Feifei GUO[c], Qifa ZHOU[d] and Lei SUN[b]**

[a]

[b]Interdisciplinary Division of Biomedical Engineering, The Hong Kong Polytechnic University, Hung Hong, Hong Kong SA

[c]National Engineering Research Center of Light Alloy Net Forming, Shanghai Jiao Tong University, Shanghai, China, 200240

[d]

[†] These authors contribute equally to this manuscript

*Corresponding Author:
Dr. Lei Sun,
Address: Room ST409, 11 Yuk Choi Road, Hung Hom, Kowloon, Hong Kong
Email: sun.lei@polyu.edu.hk
Phone: (+852)27667663

Abstract

In intravascular ultrasound (IVUS) imaging, a side-looking single element transducer is mechanically driven by a motor to rotate inside the vessel to form a 360-degree cross-sectional image. However, as the key component of IVUS system, current commercial IVUS transducers are flat and unfocused which limits the bandwidth and spatial resolution. To solve this problem, this study proposes on PMN-PT single crystal transducers with half-concave geometry for IVUS imaging. Unlike the conventional IVUS transducers with either a circular or a square flat aperture, the proposed transducer has half-concave geometric aperture which was fabricated via a mechanical dimpling technique. This unique configuration makes it possible to conduct geometric focusing at a desired depth. In this study, the conventional and the proposed IVUS transducers were designed and fabricated to evaluate and compare their acoustic properties and imaging performances. Both finite-element simulation and experimental results demonstrated that the proposed transducer has higher center frequency, broader bandwidth and better spatial resolution.

Index Term

PMN-PT single crystal; focused IVUS transducer; half-concave geometric design; mechanical dimpling technique; ultrasonic imaging

Introduction

Intravascular ultrasound (IVUS) imaging has been increasingly used for clinical investigations, since it can assess the morphological properties of blood vessels directly by cannulating a miniature catheter into the arteries.[1-3] The application of IVUS includes guiding the placement of stent, [4] or evaluation of the therapy strategies and the follow-up examinations in heart transplant recipients. [5-6] Conventionally, IVUS imaging is based on side-looking single element ultrasound transducers mechanically driven by a motor to rotate inside the vessel to form a 360 degrees cross-sectional image.[7] For clinical diagnosis purpose, superior axial resolution is required to evaluate the vulnerability of atherosclerosis especially for the thin-cap fibroatheroma. [8] However, as the key component of IVUS system, current commercial IVUS transducers are flat and unfocused with narrow bandwidths and limited spatial resolution. [9, 10]

Especially in high-resolution imaging applications, focusing is utilized to improve the lateral resolution and performance. [11-14] Shaping the piezoelectric element or using a lens is a usual way to fabricate the focusing transducers. Transducers with shaped piezoelectric element have proved to be more effective in producing high sensitivity devices as the installation of extra lens would cause attenuation due to acoustic mismatching. [15, 16] Generally, the piezoelectric transducer element is shaped by hard pressing [17, 18] or pressure defection techniques. [19] However, for side-looking IVUS transducer, the fabrication of concave surface is quite difficult. Especially, for the bulk ceramic or single crystal element, as the degradation and short-circuit may occur because the element would be broken apart during the shaping process.

This paper proposed half-concave geometric designed IVUS transducer using PMN-PT single crystal for IVUS imaging. The radiating surface of transduce is concave while the other surface remains plane. This design could be realized through the mechanical dimpling technique. [20] By mechanically grinding the single crystal, this technique can directly form a concave surface on the piezoelectric element. The thickness of piezoelectric element along the curve surface changes continuously, which causes the piezoelectric element with multi-resonances and is in favor of the bandwidth of transducer. [21] In addition, this technique can be used to fabricate focused transducers with small size and keep the piezoelectric element intact simultaneously. The acoustic properties and imaging

performance of the focused IVUS PMN-PT transducer were simulated and tested, the results were compared to conventional flat transducer. The promising results show that the half-concave geometry design will be a promising approach to build the focused IVUS transducer with broad bandwidth and good resolution and potentially capable to detect vulnerable plaque more sensitively and accurately.

Finite element simulation

A finite-element analysis software (PZFlex, Weidlinger Associates, Los Altos, CA) was used to investigate effects of half-concave geometric aperture and valuate transducer performance. Material properties used for the transducer simulation consideration are listed in Table.1.

Table.1 Material properties used for the transducer simulation.

Material	Function	c (m/s)	ρ(kg/m^3)	Z(MRayl)
PMN-0.28PT	Piezoelectric element	4640	8083	37.6
Parylene	Matching layer	2350	1100	2.58
Water	Front load	1490	1000	1.49
E-Solder 3022	Conductive backing	1850	3200	5.92

The thickness of the PMN-PT single crystal was set to be 75μm with corresponding center frequency around 30 MHz. Parylene was used for matching layer, and the thickness was set to be 24 μm based on the quarter-wavelength criterion. 1 mm E-solder 3022 backing layer was effectively achieved. At the edges of the model, absorbing boundary conditions were used. Box size was chosen to be 1/20 wavelength at radiating direction and 1/10 wavelength at other directions. During the simulation process, piezoelectric material was connected series to a 50 Ω resistor, and the transducer was excited with a single cycle of a sinusoidal signal under the following conditions: an excitation frequency of 30 MHz, a driving voltage of 1V peak-to-peak. PZFlex was used to simulate radiation patterns, and pulse-echo spectra.

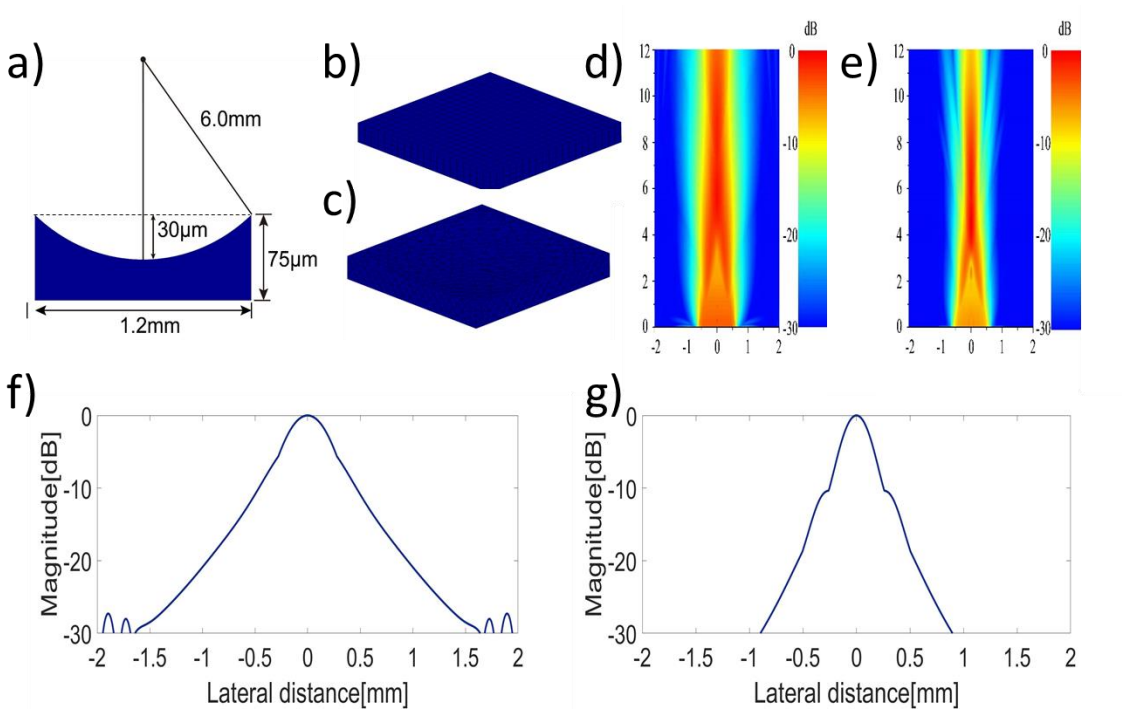

Figure.1 (a) Designed specification of the PMN-PT stack with half-concave geometry aperture; (b) & (c) structural schematic of the PMN-PT stack with flat aperture, and stack with half-concave aperture. (d) & (e) are the radiation patterns generated by the transducer with flat aperture, and transducer with half-concave geometry aperture. (f) & (g) are the on focus lateral beam profiles simulated at a depth of 9.2 mm for the flat aperture and 6 mm for the half-concave aperture.

Figure.1 shows the simulation structural schematic of the PMN-PT stack with flat aperture (Fig.1b), stack with half-concave geometry aperture (Fig.1c), and the designed specification of the dimpled PMN-PT stack (Fig.1a). The natural focal depth of the flat aperture is in the vicinity of 9.2 mm, and focal depth of the half-concave aperture is around 6 mm, which was obtained from the PZFlex simulation under the condition of a sound speed of 1490 m/s. In the simulation, the focal depth was determined when the beam intensity along the axial direction had a peak value. The -6 dB beamwidths of the flat transducer and the focusing transducer are found to be 0.58 mm and 0.35 mm, respectively. Therefore, from the simulation results, it can be observed that the dimpled transducer has a tighter focus compared with the flat transducer.

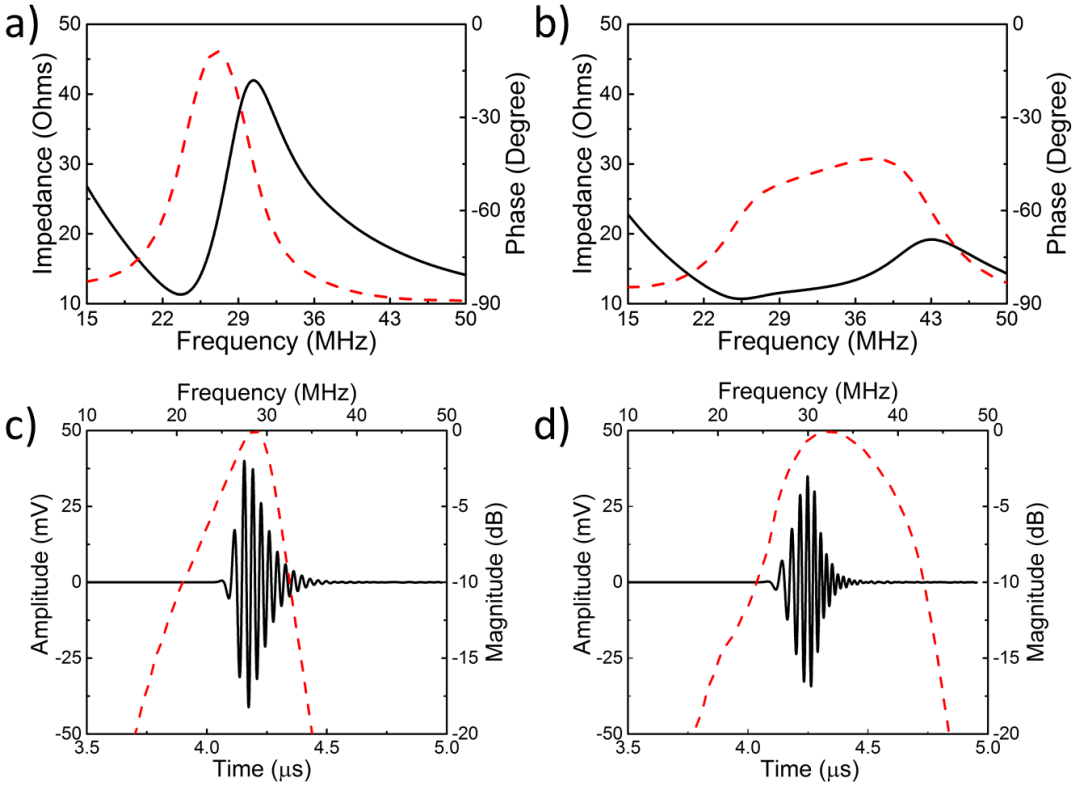

Figure.2 Simulated electrical impedance and pulse-echo waveform of the transducer with flat aperture (a) & (b) and half-concave aperture (c) & (d).

The simulated electrical impedance/phase spectra are shown in Figure.2 (a) and (c). The resonance broadens for the transducer with half concave aperture, which can be considered as resonances from various thicknesses along the curve surface of the PMN-PT stack. It is shown that the center frequency of the transducer with half concave aperture shifts to higher frequency compared to that of the flat one, which is attributed to the reduction of the crystal thickness after dimpling.

The pulse-echo waveform and frequency spectrum (Fig.2 (b) & (d)) were also achieved from the finite-element simulation. The center frequency (f_c) and -6 dB bandwidth (*BW*) were calculated to be 27.6 MHz, 28.6% for the flat transducer, and 33.6 MHz, 44.5% for the half concave one. The little higher center frequency and much broader -6 dB bandwidth can be attributed to the reduction of the thickness and the multi-resonances caused by continuous change of thickness along the curve surface of the piezoelectric element.

Materials and Methods

A. Fabrication of the IVUS Transducer with half-concave aperture

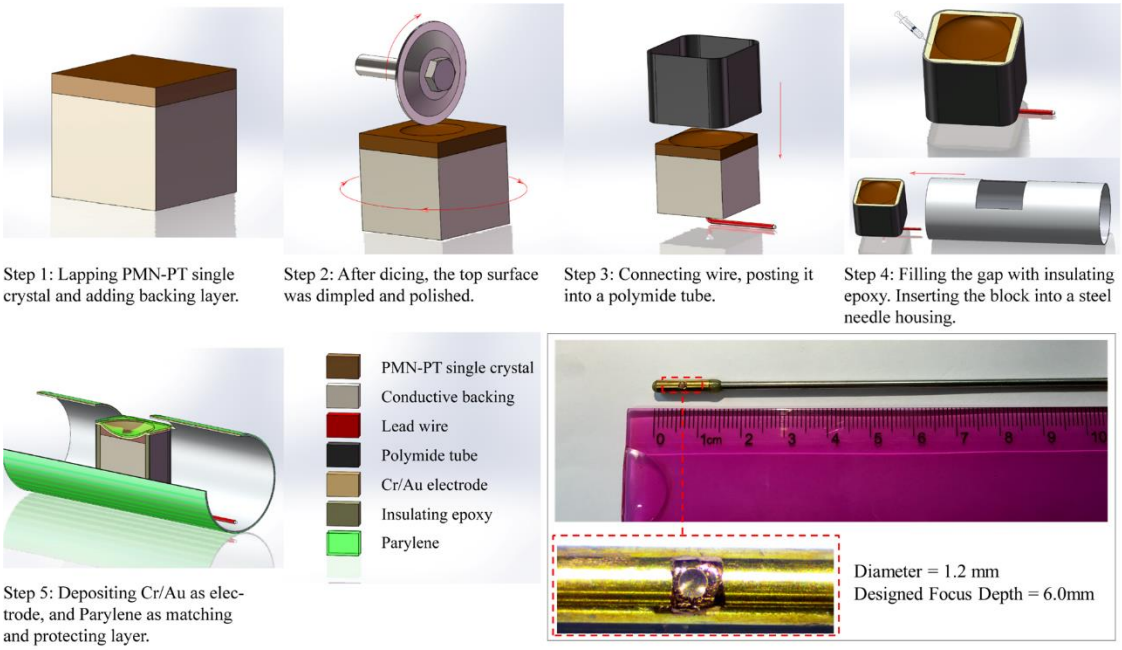

Figure.3 The schematic fabrication flow and photograph (inserted figure) of the IVUS transducer with half concave aperture.

(001)-oriented PMN-0.28PT single crystal was selected to fabricate the high performance intravascular ultrasound (IVUS) transducer because it exhibits good electromechanical coupling capability (k_t ~ 0.6), high piezoelectric constant (d_{33} ~ 1500 pC/N) and relative clamped dielectric constant ($\varepsilon^s/\ \varepsilon_0$ ~ 940), which makes it an idea material for designing high sensitivity single element transducer. [22] The fabrication process as well as the photograph of the focused PMN-PT transducer are shown in Figure.3. The fabrication process is as follows. The PMN-PT single crystal was first lapped to around 75 μm, then Cr/Au (50/100 nm) electrodes were sputtered on one side of the PMN-PT. E-solder 3022 (VonRoll Isola, New Haven, CT) was cast on one side as the backing material and lapped to 2 mm. The sample was then diced to 1.2*1.2 mm^2 posts using dicing saw (Tcar 864-1, Thermocarbon, Casselberry, FL). In order to shape a focused piezoelectric element, the opposite side of the PMN-PT single crystal was dimpled using a dimple grinder (model 656, Gatan). The focal length of the element was controlled by the diameter of the grinding wheel (12 mm in this experiment). For transducers with 30 MHz design

frequency, the diameter of concave was chosen as 1.2 mm. After that, the 1.2*1.2 mm^2 post was housed inside a polyimide tube with an inner diameter of 1.7 mm. A lead wire was connected to the backing layer with an additional amount of conductive epoxy. The polyimide tube provided electrical isolation from the steel housing. A layer of Cr/Au (50 nm/100 nm) was sputtered across the transducer face to form the ground plane connection. Finally, a thin layer of parylene (~ 24 μm) was vapor-deposited by a PDS 2010 Labcoator (Specialty Coating Systems, Indianapoils, IN) on the front face of the transducer, serving as an acoustic matching layer and a protection layer. For comparison, the flat transducer with aperture of 1.2 mm was also fabricated using the same process.

B. Experiment details for Performance Evaluation

The frequency dependence of electrical impedance and phase plots was measured by WK6500B 1J65120B impedance analyzer (Wayne Kerr Electronics, UK).

The conventional pulse-echo response measurement was carried out in distilled water, in which the transducer was connected to a JSR Ultrasonics DPR 500 (Imaginant, Pittsford, NY) pulser/receiver and excited by an electrical impulse at 200 Hz repetition rate and 50 Ω damping. The energy involved was 2.3 μJ and no gain was applied. The echo response was captured and displayed on an oscilloscope (Infinium 54810A, HP/Agilent, USA), the built-in fast Fourier transform (FFT) feature of the oscilloscope was used to compute the frequency spectrum of the pulse-echo response. An X-cut quartz plate was used as a reflector.

To measure the insertion loss (IL), the transducer was connected to a function generator (AFG2020 function generator, Tektronix, Inc., Beaverton, OR) which was used to generate a tone burse of 20-cycle sine wave at center freuqnecy. The echo signal received by the transducer was measured by the oscilloscope with 1 MΩ coupling. The amplitude of the driving signal was measured with 50 Ω. The following equation was used for calculation:

$$\mathrm{IL} = 20log_{10}(V_0/V_i) + 1.9 + 2.2 \times 10^{-4} \times 2d \times f_c^2$$

Where IL means the insertion loss, V_i and V_o are input and output voltage amplitudes, respectively; d is the distance from the transducer to the quartz target in millimeters. The

signal loss resulted from transmission into quartz was compensated by 1.9 dB and 2.2 X 10^{-4} dB/mm·MHz^2 due to the attenuation in water.

To compare the spatial resolution of the IVUS transducers, imaging of a custom-made wire phantom consisting of six 30 μm tungsten wires was acquired. The wire phantom was immersed into the container on a stage with separation distance of 0.5 mm at Z direction. Customized high frequency ultrasonic imaging system was used to transmit and receive echo signal. [23-25] Then B-mode images of wire phantoms were generated and processed using MATLAB program.

The acoustic pressure maps were acquired by a 3D ultrasound intensity measurement system (UMS3, Precision acoustics, Dorchester, UK). IVUS transducers and needle hydrophone ((SN2010, 0.5 mm probe, Precision acoustics, Dorchester, UK) were placed oppositely in degassed water. The IVUS transducers were driven at their center frequency using function generator combined with RF power amplifier (A075, E&I, Rochester, N.Y., USA). The signals from the hydrophone were captured by a digital oscilloscope (DSOX3024A, Agilent, USA), then plotted in a pseudo-color using the MATLAB program.

Results

A. Characterization of the IVUS Transducers

The frequency dependence of electrical impedance and phase plots is displayed in Figure.4 (a) & (b). As can be seen from the plots, the resonant frequency of the focusing transducer shifts higher compared to that of the flat one and there exist two weak resonance peaks which may be attributed to the reduction and variation of the crystal thickness after dimpling. The pulse-echo response and frequency spectra of IVUS transducers are shown in Figure.4 (c) & (d), the center frequency (f_c) and -6 dB bandwidth (*BW*) were acquired from the frequency spectra, which were calculated to be 32 MHz, 28% for flat transducer, and 35 MHz, 54% for the half-concave one. The little higher center frequency and much broader -6 dB bandwidth can be attributed to the multi-resonances caused by continuous change of thickness along the curve surface of the dimpled piezoelectric element. The measured transducer performance was summarized in Table.2.

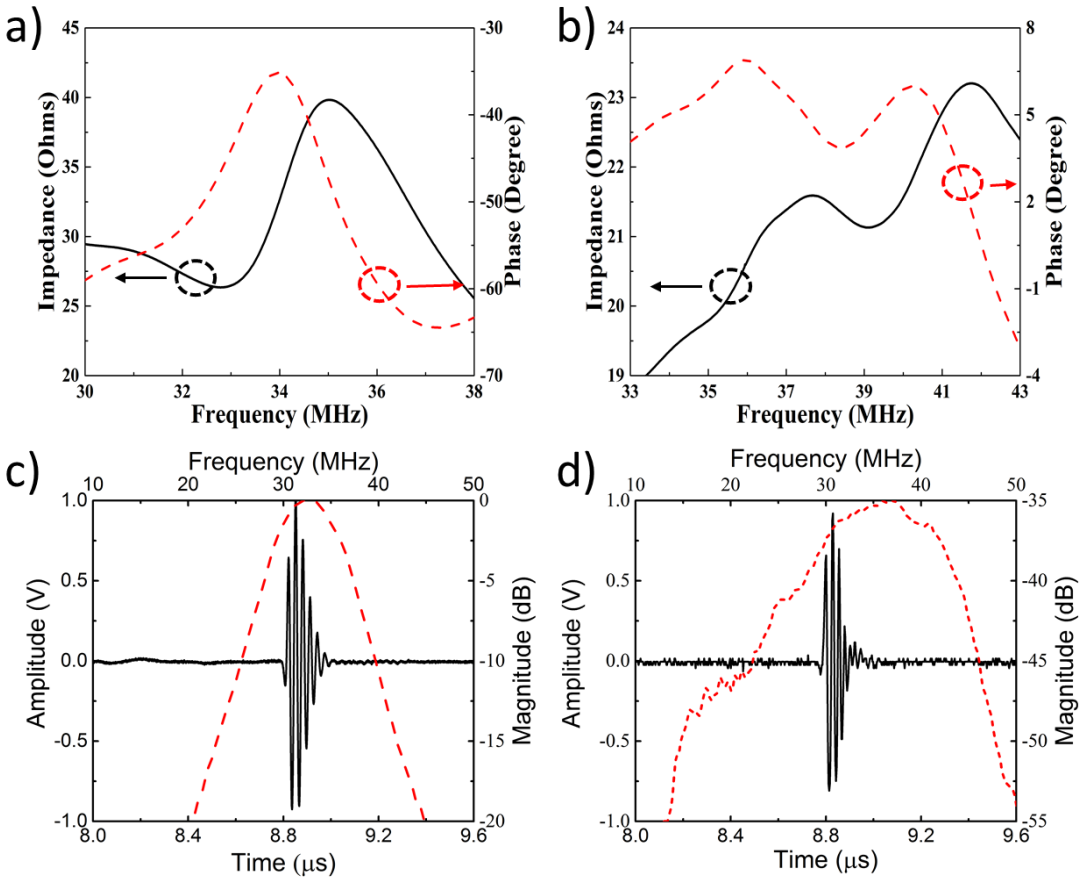

Figure.4 Electrical impedance and phase plots of IVUS transducers (a) with flat aperture, (b) with half-concave aperture; the pulse-echo response and frequency spectra of IVUS transducers (c) with flat aperture and (d) with half-concave aperture.

Table.2 Measured transducer performance

Properties	Flat	Half-concave
Center Frequency (MHz)	32	35
-6 dB Bandwidth	28%	54%
-6 dB Pulse Length (ns)	90	46
Aperture (mm)	1.2*1.2	Φ1.2
Focus Depth (mm)	\	6.6

The insertion loss of half-concave transducer was measured to be -22.4 dB at 35 MHz compared with flat one (IL = -19.3 dB at 32 MHz). The increase of *IL* for half-concave transducer may be due to the unused corner of the piezoelectric element compared with the flat one, or may because of the nonuniform thickness of PMN-PT single crystal which causes different mode of vibration and brings excess energy loss.

B. Comparison of the Spatial Resolution

Figure.5 (a) & (b) show the images of 30 μm wire phantom from the flat and the half-concave transducer, respectively. Under visual assessment, it was easy to recognize that the lateral resolution of half-concave transducer was superior to that of the flat one. For the flat transducer, the signal weakens over imaging distance though, leads to the decrease of contrast resolution. However, for the half-concave transducer, the contrast resolution remains relatively high level in a wide range around the focus area. To ascertain this, pressure measurements were performed, and illustrated in Figure. 5 (c) & (d). The results are in accordance with those shown in images of 30 μm wire phantom. The lateral resolution of half-concave transducer obtained from -6 dB envelope width was 392 μm at 6.5 mm, and the lateral resolution of flat transducer was 810 μm at 4 mm as shown in Figure. 5 (e). The lateral resolution of focused transducer was improved like the PZFlex simulations results. The axial resolution was calculated from the FWHM of the pulse length of the echo, which was 34.5 μm and 67.5 μm for the half-concave and flat transducers, respectively.

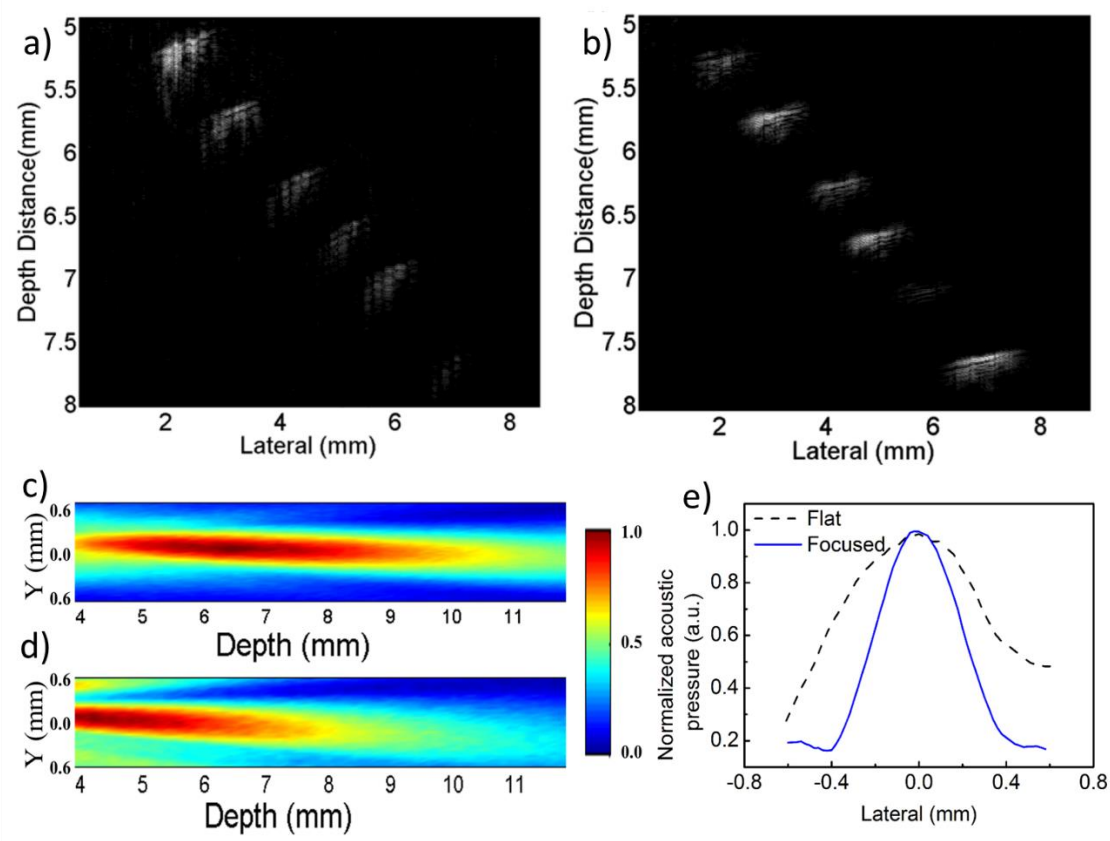

Figure.5 The image of 30 μm wire phantom for the (a) flat and (b) half-concave transducers. Measured radiation patterns for (c) flat and (d) half-concave transducers. (e) Normalized acoustic pressure vs lateral diameter for IVUS transducers.

Discussions and Conclusion

In this paper, we proposed an IVUS transducer with half-concave geometry design and ascertained that the half-concave aperture is capable of improving -6 dB bandwidth and lateral resolution. Unlike a circular or a square flat aperture of the conventional IVUS transducers, the half-concave geometric aperture of the proposed transducer was fabricated via a mechanical dimpling technique. This unique configuration makes it possible to conduct geometric focusing at a desired depth. The benefits of a half-concave aperture for both -6 dB bandwidth and lateral resolution were verified by the simulation and experiments in this study.

Due to the dimpling process, the thickness along the curve surface continuously changes, leads to multi-resonances around the center frequency, which benefits the

improvement of -6 dB bandwidth. The reduction of the crystal thickness makes the center frequency shaft to higher frequency. All these factors make the half-concave transducer have better spatial resolutions than the flat one. However, the insertion loss of the half-concave transducer at center frequency is around 3 dB larger than the flat one, which may be also caused by the operation of PMN-PT piezoelectric elements. As illustrated in wire phantom imaging and pressure measurement, the half-concave geometric design avoids the disadvantage of the flat one in which the signal weakens over imaging distance though and improves the imaging quality to some extent.

All in all, the half-concave aperture design via mechanical dimpling method could increase the center frequency of the transducer, broaden the -6 dB bandwidth, sharpen the focus, as a result, the spatial resolution of transducer could be improved significantly. Side effect of the dimpling process is that, the sensitivity will be degenerated slightly. Such half-concave aperture may make the side-looking focused transducers promising for IVUS imaging. Also, we should realize that, in the case of a small, as the region of interest becomes shallower, the focal length should be decreased. It will be necessary to reduce the aperture size and try to focus at closer distance. It is also desirable to increase an operating frequency in order to achieve higher spatial resolution. Consequently, it is possible to satisfy the requirements for the proposed method through fine processing.

Acknowledgement

Financial support from the Hong Kong Innovation and Technology Fund (ITS/059/15 and ITS/053/16), Health and Medical Research Fund (01121836), and National Natural Science Foundations of China (61372026) are greatly appreciated.

References

[1] S. J. Nicholls, I. Sipahi, P. Schoenhagen, T. Crowe, E. M. Tuzcu, and S. E. Nissen, “Application of intravascular ultrasound in anti-atherosclerotic drug development,” Nat Rev Drug Discov., vol. 5, no.6, pp. 485-492, 2006.

[2] C. L. de Korte, A. F. W. van der Steen, E. I. Cespedes, G. Pasterkamp, S. G. Carlier, F. Mastik, A. H. Schoneveld, P. W. Serruys, and N. Bom, “Characterization of plaque components and vulnerability with intravascular ultrasound elastography,” Phys. Med. Biol., vol. 45, no. 6, pp. 1465-1475, 2000.

[3] M. Hartmann, J. Huisman, D. Bose, L. O. Jensen, P. Schoenhagen, G. S. Mintz, R. Erbel, and C. von Birgelen, “Serial intravascular ultrasound assessment of changes in coronary atherosclerotic plaque dimensions and composition: an update,” Eur J Echocardiogr., vol. 12, no. 4, pp. 313-321, 2011.

[4] P. A. Lemos, F. Saia, J. M. R. Ligthart, et al., “Coronary restenosis after sirolimus-eluting stent implantation: morphological description and mechanistic analysis from a consecutive series of cases,” Circulation, vol. 108. No. 3, pp. 257-260, 2003.

[5] J. A. Kobashigawa1, J. M. Tobis, R. M. Mentzer, H. A. Valantine, R. C. Bourge, M. R. Mehra, F. W. Smart, L. W. Miller, Koji Tanaka, Haiyan Li, D. W. Gjertson, and R. D. Gordon, “Mycophenolate mofetil reduces intimal thickness by intravascular ultrasound after heart transplant: reanalysis of the multicenter trial,” Am J Transplant.， vol. 6, no. 5p1, pp. 993-997, 2006.

[6] J. A. Kobashigawa, J. M. Tobis, R. C. Starling, E. M. Tuzcu, A. L. Smith, H. A. Valantine, A. C. Yeung, M. R. Mehra, H. Anzai, B. T. Oeser, K. H. Abeywickrama, J. Murphy, and N. Cretin, “Multicenter intravascular ultrasound validation study among heart transplant recipients: outcomes after five years,” J Am Coll of Cardiol., vol. 45, no. 9, pp. 1532-1537, 2005.

[7] F.S. Foster, C.J. Pavlin, K.A. Harasiewicz, D.A. Christopher, and D.H. Turnbull, “Advances in ultrasound biomicroscopy,” Ultrasound Med. Biol., vol. 26, no. 1, pp. 1-27, 2000.

[8] R. Virmani, A.P. Burke, J.T. Willerson, A. Farb, J. Narula, and F.D. Kolodgie, "The pathology of vulnerable plaque. The Vulnerable Atherosclerotic Plaque: Strategies for Diagnosis and Management,"pp. 21-36, 2007.
[9] X. Li, W. Wu, Y. Chung, W.Y. Shih, W.H. Shih, Q.F. Zhou, and K.K. Shung, "80-MHz intravascular ultrasound transducer using PMN-PT free-standing film," IEEE Trans. Ultrason. Ferroelectr. Freq. Control., vol. 58, no. 11, pp. 2281-2288, November 2011.
[10] C. Chandrana, N. Kharin, G.D. Vince, S. Roy, and A.J. Fleischman, "Demonstration of second-harmonic IVUS feasibility with focused broadband miniature transducers," IEEE Trans. Ultrason. Ferroelectr. Freq. Control., vol. 57, no. 5, pp. 1077-1085, May 2010.
[11] Q.F. Zhou, C. Sharp, J.M. Cannata, K.K. Shung, G.H. Feng, E.S. Kim, "Self-focused high frequency ultrasonic transducers based on ZnO piezoelectric films," Appl. Phys. Lett, 90 p. 113502, 2007.
[12] P. Marechal, F. Levassort, L.P. Tran-Huu-Hue, M. Lethiecq, "Lens-focused transducer modeling using an extended KLM model," Ultrasonics, 46, pp. 155–167, 2007.
[13] E. Herbert, M. Pernot, B. Larrat, G. Montaldo, M. Tanter and M. Fink, "Energy-based adaptive focusing of waves: application to ultrasonic imaging and therapy," in: Proc. IEEE on Ultra. Symp. 2008, pp. 875–878.
[14] Y. Hertzberg, A. Volovick, Y. Zur, Y. Medan, S. Vitek, G. Navon, "Ultrasound focusing using magnetic resonance acoustic radiation force imaging: application to ultrasound transcranial therapy," Med. Phys, 37, pp. 2934–2942, 2010.
[15] J. M. Cannata, T. A. Ritter, W. H. Chen and K. K. Shung, "Design of focused single element (50–100 MHz) transducers using lithium niobate," in: Proc. IEEE on Ultra. Symp. 2000, pp. 1129–1133.
[16] K.A. Snook, J.Z. Zhao, C.H.F. Alves, J.M. Cannata, W.H. Chen, J.J. Meyer, T.A. Ritter, K.K. Shung, "Design, fabrication, and evaluation of high frequency, single-element transducers incorporating different materials," IEEE Trans. Ultrason. Ferroelectr. Freq. Control, 49, pp. 169–176, 2002.
[17] J. H. Liu, S. Y. Chen and P. C. Li, "Design and fabrication of a 40 MHz transducer with enhanced bandwidth," in: Proc. IEEE on Ultra. Symp. 2008, pp. 799–802.
[18] C.H. Chung, Y.C. Lee, "Broadband poly(vinylidenefiuoride–trifiuoroethylene) ultrasound focusing transducers for determining elastic constants of coating materials," J.

Nondestruct. Eval, 28, pp. 101–110, 2009.
[19] C. Chandrana, N. Kharin, G.D. Vince, S. Roy, A.J. Fleischman, “Demonstration of second-harmonic IVUS feasibility with focused broadband miniature transducers,” IEEE Trans. Ultrason. Ferroelectr. Freq. Control, 57, pp. 1077–1085, 2010.
[20] K.H. Lam, Y. Chen, K.F. Cheung, J.Y. Dai, “PMN–PT single crystal focusing transducer fabricated using a mechanical dimpling technique,” Ultrasonics, 52, pp. 20–24, 2012.
[21] J. Chen, J.Y. Dai, C. Zhang, Z.T. Zhang, and G.P. Feng, “Bandwidth improvement of LiNbO3 ultrasonic transducers by half-concaved inversion layer approach,” Rev. Sci. Instrum., vol. 83, pp. 114903, 2012.
[22] Q. Zhou, X. Xu, E. J. Gottlieb, L. Sun, J. M. Cannata, H. Ameri, M. S. Humayun, P. Han, and K. K. Shung, “PMN-PT single crystal, high-frequency ultrasonic needle transducers for pulsed-wave Doppler application,” IEEE Trans. Ultrason. Ferroelectr. Freq. Control, vol. 54, no. 3, pp. 668-675, 2007.
[23] Qiu W, Chen Y, Yu Y, Cheng WF, Tsang FK, Dai J, Shung KK, Zhou Q, Sun L. An open system for intravascular ultrasound imaging. IEEE Transactions on Ultrasonics Ferroelectrics Frequency Control 2012;59(10):2201-2210.
[24] Qiu W, Yu Y, Tsang FK, Sun L. A multi-functional, reconfigurable pulse generator for high frequency ultrasound imaging. IEEE Transactions on Ultrasonics Ferroelectrics Frequency Control 2012;59(7):1558-67.
[25] Qiu W, Yu Y, Tsang FK, Sun L. An FPGA based open platform for ultrasound biomicroscopy. IEEE Transactions on Ultrasonics Ferroelectrics Frequency Control 2012; 59(7):1432-42.